Carbohydrate Polymers 115 (2015) 485–493

Contents lists available at ScienceDirect

Carbohydrate Polymers

journal homepage: www.elsevier.com/locate/carbpol

Tissue engineering scaffolds electrospun from cotton cellulose

Xu He [a], Long Cheng [a], Ximu Zhang [b], Qiang Xiao [b], Wei Zhang [a,*], Canhui Lu [a,*]

[a] State Key Laboratory of Polymer Materials Engineering, Polymer Research Institute at Sichuan University, Chengdu 610065, China
[b] State Key Laboratory of Oral Disease, West China Hospital of Stomatology, Sichuan University, Chengdu 610041, China

ARTICLE INFO

Article history:
Received 27 November 2013
Received in revised form 25 August 2014
Accepted 26 August 2014
Available online 19 September 2014

Keywords:
Cellulose nanofibers
Electrospinning
Fiber alignment
Mechanical properties
Tissue engineering

ABSTRACT

Nonwovens of cellulose nanofibers were fabricated by electrospinning of cotton cellulose in its LiCl/DMAc solution. The key factors associated with the electrospinning process, including the intrinsic properties of cellulose solutions, the rotating speed of collector and the applied voltage, were systematically investigated. XRD data indicated the electrospun nanofibers were almost amorphous. When increasing the rotating speed of the collector, preferential alignment of fibers along the drawing direction and improved molecular orientation were revealed by scanning electron microscope and polarized FTIR, respectively. Tensile tests indicated the strength of the nonwovens along the orientation direction could be largely improved when collected at a higher speed. In light of the excellent biocompatibility and biodegradability as well as their unique porous structure, the nonwovens were further assessed as potential tissue engineering scaffolds. Cell culture experiments demonstrated human dental follicle cells could proliferate rapidly not only on the surface but also in the entire scaffold.

1. Introduction

Cellulose, categorized as a linear polysaccharide and the most abundant natural resource on earth (Ma et al., 2013), is a rapidly renewable biopolymer with a long history in fiber manufacturing (Hon, 1994; Frey, 2008). It has excellent advantages of world-wide availability, biodegradability and sustainability, making it widely used in packaging, textiles and biomedical materials (Nishio, 2006; Mahmoudian, Wahit, Ismail, & Yussuf, 2012). Particularly, the biocompatibility and the low water solubility of cellulose allow for good control over scaffold design (Müller et al., 2006). In vivo applications of cellulose-based materials have demonstrated only negligible inflammatory response reactions (Fricain et al., 2002; Czaja, Young, Kawecki, & Brown, 2007).

Electrospinning is a unique processing technique that can be used to fabricate ultra-fine fibers with diameters in the range of micrometer down to nanometer (<100 nm) through a high voltage charged polymer solutions or melts (Reneker & Yarin, 2008). During the past decade, electrospinning has attracted much attention in tissue engineering. It generates thin, continuous polymer fibers with micro to nanoscale topography and high porosity (>90%) similar to the natural extracellular matrix (ECM), and promotes cellular interactions resulting in new tissue formation (Sill & von Recum, 2008; Jose, Thomas, Johnson, Dean, & Nyairo, 2009; Rnjak-Kovacina, Wise, Li, Maitz, & Young, 2011). However, electrospun nonwoven mats usually exhibit poor mechanical performance, representing one of the limitations for the materials (Sehaqui, Morimune, Nishino, & Berglund, 2012). For many applications such as protecting cloth, battlefield dressings and tissue engineering scaffolds, mechanical strength and toughness of the electrospun fibers are extremely important as even partial failure could have dire consequences (Blond et al., 2008). Previously, Thomas et al. (2006) reported the scaffold of electrospun polycaprolactone (PCL) nanofibers could achieve a high degree of orientation and alignment when collected on a fast rotating drum, leading to several-fold increase of the mechanical properties along the fiber orientation direction.

Although there have already been numerous studies on electrospun nanofibers from various polymers, electrospinning of native cellulose has rarely been conducted mainly due to the difficulties encountered during this process (Schiffman & Schauer, 2008; Rodríguez, Gatenholm, & Renneckar, 2012). Cellulose cannot be directly dissolved in common solvents owing to its high crystallinity enhanced by tremendous hydrogen bonding network (Wang et al., 2013). Therefore, most studies of cellulose electrospinning were based on cellulose derivatives (Frey, 2008; Du & Hsieh, 2009), though the resultant electrospun fibers were very weak with tensile strength usually less than 1 MPa (Suwantong, Opanasopit, Ruktanonchai, & Supaphol, 2007). There are limited solvents that can dissolve cellulose (Jayaramudu et al., 2013). Only a

* Corresponding authors at: State Key Laboratory of Polymer Materials Engineering, Polymer Research Institute at Sichuan University, Chengdu 610065, China. Tel.: +86 28 85460607; fax: +86 28 85402465.
E-mail addresses: weizhang@scu.edu.cn (W. Zhang), canhuilu@263.net (C. Lu).

http://dx.doi.org/10.1016/j.carbpol.2014.08.114
0144-8617/

few of them, such as *N*-methyl-morpholine *N*-oxide solution/water (NMMO/H_2O), lithium chloride/dimethyl acetamide (LiCl/DMAc) and ionic liquids can be applied for electrospinning because of the dielectric requirements of the technique (Magalhães, Cao, & Lucia, 2009).

The objective of this work was to develop mechanically robust electrospun nanofiber nonwovens from cotton cellulose and evaluate their potentials in tissue engineering applications. In order to cope with the poor mechanical properties, the cellulose nanofibers were uniaxially aligned using a rotating drum as the collector. The solvent system of LiCl/DMAc, which only causes negligible degradation of cellulose (Dupont, 2003), was adopted for electrospinning of non-derivative cellulose. The key factors associated with the electrospinning process, including conductivity, viscosity, surface tension of the cellulose solutions and the applied voltage were discussed. The morphological and structural development of electrospun fibers induced by the rotating collector, such as fiber alignment, molecular orientation and crystallinity were comprehensively investigated. Moreover, the mechanical and thermal properties of the electrospun cellulose nonwovens were studied (Sehaqui et al., 2012). In addition, the proliferation of cultured cells on the scaffolds was explored and the cell morphology was revealed by SEM and confocal laser scanning microscopy (CLSM).

2. Experimental

2.1. Materials

Purified cotton (Xuzhou Health Materials Co., Ltd) was used as the raw material. Analytical grade *N*,*N*-dimethylacetamide (DMAc) and lithium chloride (LiCl) were purchased from Chengdu Kelong Chemical Plant. For cell culture study, Dulbecco's modified eagle's medium (DMEM), trypsin, fetal bovine serum (FBS), 40,6-diamidino-2-phenylindole (DAPI) were purchased from Sigma Chemical Co. (St. Louis, MO, USA). Alexa-fluor 568 antibodies were purchased from Invitrogen (Molecular probes, Carlsbad, CA, USA). Glutaraldehyde solution (25%, in weight) was obtained from Zhongshan Fine-Chem Ltd. (Guangdong, China). All the other reagents used were of analytical grade and were used without further purification. Distilled water was used throughout the experiment.

2.2. Preparation of spinning solution

An activation pretreatment prior to cellulose dissolution was needed to weaken the polymer chain interaction to get a relaxed conformation. Natural cellulose, especially cotton cellulose, possesses very high molar mass and crystallinity. The activation pretreatment was able to enhance the diffusion kinetics of the solvent to the tightly packed crystalline regions that are less accessible. Without this pretreatment, cellulose cannot be dissolved even after a long time. Generally, there were two main methods for the activation of cellulose, known as high temperature activation and polar medium exchange activation (Dupont, 2003). It was discovered that cellulose degraded notably when submitted to high temperature activation, while polar medium exchange activation gave rise to better, faster and more reproducible subsequent dissolution with almost no degradation (Dupont, 2003). In this study, the solvent exchange method was adopted. This pretreatment included the following processes: first, immerse the cellulose in water for 1 h, and subsequently remove the water by vacuum filtration; second, exchange with methanol for 1 h to expel the residual water, and remove the methanol by vacuum filtration; third, exchange with DMAc for 1 h to get rid of the residual methanol; finally, the cellulose was vacuum filtrated and dried at 70 °C.

LiCl was very hygroscopic and thus was easy to bring water in the solvents. However, water will promote polymer aggregation and hinder the dissolution of cellulose (Potthast et al., 2002). To exclude water, LiCl was oven-dried at 110 °C and stored in a desiccator. To prepare 8% LiCl/DMAc solvent, DMAc was heated to 105 °C to expel any residual water. Then, 8 g dry LiCl was added to 92 g warm DMAc (80 °C) under magnetic stirring. After 30 min or so, LiCl was completely dissolved to form a transparent mixed solvent. The solvent was then cooled down to room temperature for use.

In this study, solutions with various cellulose concentrations ranging from 0.5% to 3% (in weight) were prepared. A typical preparation of 1% cellulose solution was as follows: 1 g activated cellulose was added to 99 g as-prepared LiCl/DMAc solvent and stirred at room temperature until complete dissolution.

2.3. Electrospinning

The flow rate of the micropump and the tip-to-collector distance can be precisely controlled by a computer, which was connected to the electrospinning equipment (FM-12, Beijing Fuyouma Technology Co.). Parameters such as the applied voltage, the tangential velocity, and the temperature can be manually adjusted from the control panel on the equipment. The electrospinning was carried out at room temperature. A metallic rotating collector wrapped with aluminum foil was placed 10 cm away from the tip of the nozzle to collect fibers. Electrospinning of cellulose solutions was conducted over a wide range of electric field strengths by varying the voltage drop for a preset distance. The flow rate was set at 0.03 mL/min. The rotating collector was partly immersed in water, which was used as the coagulation bath in order to obtain dimensionally stable fibers and to remove DMAc and LiCl. Note that water could be splashed out from the container if most of the rotating collector was immersed in the coagulation bath. Herein, only the bottom part of the collector (approximately 10 mm) was immersed in water and the water was not splashed out at least at the rotating speeds applied. Samples were subsequently dried under ventilation and then kept sealed.

2.4. Seeding of hDFCs on scaffolds

Primary human dental follicle cells (hDFCs) were obtained from patients aged 14 and 20 years after obtaining informed consent as reported previously (Morsczeck et al., 2005). Briefly, normal human impacted third molars were surgically removed and collected. Dental follicle tissues were digested in a solution of 0.1 U/mL collagenase type I and 1 U/mL dispase (Roche, Mannheim, Germany) for 1 h at 37 °C. Attached hDFCs were cultured at 37 °C in 100-mm dishes using MSC growth medium (GM; consisting of MSC basal medium supplemented with fetal bovine serum, L-glutamine and penicillin/streptomycin; Lonza, Walkersville, MD) in a humidified incubator (CO_2 incubator MCO-175M; Sanyo, Osaka, Japan) with the presence of 5 vol% CO_2 in air at 37 °C. In this study, passage 3 to 5 hDFCs were used. The morphology of obtained hDFCs seeds was observed using an optical microscopy (UB200i, Chongqing UOP photoelectric technology Co., Ltd, China).

The cellulose nanofiber scaffolds used in this study were about 0.05 mm in thickness and were cut into discs of 13 mm in diameter. Before seeding cells, the scaffolds were dehydrated by passing them through ethanol with gradient concentrations (20%, 40%, 60%, 80% and 100%, v/v) for the duration of 15–20 min for each concentration. Subsequently, in order to remove the traces of ethanol, scaffolds were washed in 0.1 M PBS (pH 7.4) three times (5 min for each wash). Scaffolds were then treated with UV to ensure the proper sterilization. For appropriate cell attachment, scaffolds were saturated in complete DMEM by incubating them in 1 mL media for 1 h (Bhat & Kumar, 2012). Then, 0.5 mL cell suspension was seeded at

variable densities depending on the type of experiment, followed by the incubation of the scaffolds at 37 °C in 5 vol% CO_2 at 80–90% humidity. Seeding was done on both sides of the samples. Samples were removed at specific intervals for the examination of cell proliferation via SEM and CLSM.

2.5. Characterization

The morphology of the electrospun fibers was observed by field emission scanning electron microscope (JEOL, JSM-7500F). Surface tension of cellulose/LiCl/DMAc solutions was measured by a surface tension meter (KRUSS GmbH Germany, K100C-MK2). Conductivity of cellulose solutions was measured by a conductivity meter (DDS-11A, Chengdu Century Ark Technology Co.). Fiber diameter was measured from SEM images with the software Smileview (at least 100 fibers were chosen). The viscosity measurement of cellulose solutions was conducted in an oscillatory mode on a rheometer (Gemini 200 rheometer, Bohlin Co., UK) equipped with a parallel plate geometry using 25 mm diameter plates at room temperature (20 °C). Polarized FTIR transmission measurement was performed on a Nicolet 560 spectrophotometer (USA). Nonwovens (about 20 μm in thickness) were used for the test. Wide angle X-ray diffraction (WAXD) analysis was performed on a Philips Analytical X'Pert X-diffractometer (Philips Co., Netherlands), using Cu-$K\alpha$ radiation ($\lambda = 0.1540$ nm) at an accelerating voltage of 40 kV and the current of 40 mA. The data were collected from $2\theta = 5$–50° with a step interval of 0.03°. Raman spectra were recorded on a Raman spectrometer (LabRAM HR, HORIBA Jobin Yvon S.A.S.) at 2 cm^{-1} resolution with 200 scans. Factor analysis was performed on the materials in the range of 200–1200 cm^{-1}. Tensile strength measurement was conducted on a tensile testing machine (LLY-06E/PC, Laizhou Electron Instrument Co.). Nonwoven mats were cut by length (along the fiber long axis) and width (perpendicular to the fiber long axis) with dimensions of 60 mm × 2 mm × d, where d is the thickness of the nonwovens. The stretching rate was maintained at 1 mm/min. Tensile strength was calculated by dividing the maximum load at break by the initial specimen's cross-sectional area. The cross-sectional area was defined by the thickness multiplied by the width of sample (2 mm here). The samples' thickness was measured using a digital micrometer (MC03000002, Guilin Guanglu Measuring Instrument Co., China) and the result was expressed as the average of 5 random measurements of the sample. Before testing, all specimens were equilibrated in a chamber kept at 25 °C and 50% relative humidity for 4 days. Each test trial per film consisted of 5 replicate measurements. TGA was performed with a TG209 F1 instrument (NETZSCH Co., Germany) to measure the decomposition temperature of the electrospun fibers. The samples were heated from 40 to 600 °C at a heating rate of 10 °C/min under a nitrogen gas flow (100 mL/min).

hDFCs cultured on the cellulose scaffolds were examined by SEM. Scaffolds (seeded with hDFCs, cultured for 4 days) were removed from the growth media, followed by the gentle washing with sterile PBS 0.1 M. Cells were fixed on the surface of the scaffold with 2.5 wt% glutaraldehyde in 0.1 M sodium cacodylate for 4.5 h at 4 °C. Scaffolds were then dehydrated through a series of alcohol from 20 to 70 vol%, stained in 0.5 wt% uranyl acetate, followed by further dehydration in 90, 95, and 100 vol% alcohol. The final dehydration was followed by drying in a vacuum desiccator. Then the samples were sputter coated with gold before SEM imaging (S-4500; Hitachi, Japan) at an accelerating voltage of 20 kV.

hDFCs grown on the cellulose scaffolds were observed by CLSM. After 4 days culture, analysis media was aspirated and scaffolds were gently washed with cold PBS. Fixation of the cell-scaffold samples was carried out for 20 min in freshly prepared 2 vol% paraformaldehyde. Then the samples were washed in cold PBS three times, permeabilized in PBS containing 10 vol% FBS plus 0.5 vol% Triton-X 100 (Sigma Aldrich, St. Louis, MO, USA) for 20 min, and incubated in PBS containing 10 vol% FBS for 30 min. Thereafter, samples were stained with Alexa-fluor 568 conjugated phalloidin for filamentous actin fluorescence (1:200) and cell nuclei were marked by 40,6-diamidino-2-phenylindole (DAPI) staining for nuclei UV–visualization (1:2000) for 2 h. Subsequently, specimens were thoroughly washed with PBS, and rinsed with deionized water for 2 min. Finally specimens were visualized using an Olympus FV1000 confocal laser scanning microscope (Olympus, Tokyo, Japan) at 460 nm (emission) and the multi-track images were captured with a 60×/1.35 NA objective.

3. Results and discussions

3.1. Factors influencing the electrospinning process

The intrinsic solution properties were deemed as important factors which would strongly influence the electrospinning process. These solution properties at different cellulose concentrations, including conductivity, viscosity, surface tension and spinnability, were listed in Table 1. The diameters of the electrospun fibers, which were prepared at the applied voltage of 20 kV and the tip-to-collector distance of 10 cm, were also presented. The conductivity and surface tension increased with the increase of cellulose concentration. The solution with 0.5% cellulose concentration cannot be electrospun. It just dripped off the needle without continuous fibers formed on the collector. Many factors could affect the electrospinning process, such as temperature, type of solvent, molecular weight of polymer, conductivity, viscosity and surface tension of solution, tip-to-collector distance, applied voltage, and flow rate (Greiner & Wendorf, 2007). In the present study, the viscosity of 0.5% cellulose solution (0.1 Pa s at the shear rate of 0.01 s^{-1}) was much lower than those for 1%, 1.5% and 2% cellulose solution (39.73, 88.95, 390.5 Pa s at the shear rate of 0.01 s^{-1}, respectively). We believe the very low viscosity of the 0.5% cellulose solution should be mainly responsible for its non-electrospinnability. On the contrast, cellulose solutions with concentrations from 1% to 2% can be well electrospun. The average fiber diameter increased from 220 nm (1%) to 280 nm (2%). However, when cellulose concentration went up to 3%, the solution was non-electrospinnable again

Table 1
The intrinsic properties of cellulose solutions.

Concentration of cellulose (%)	Viscosity (Pa s)	Conductivity (mS/cm)	Surface tension (mN/m)	Spinnability	Fiber diameter (nm)	Average fiber diameter (nm)
0.5	0.1	0.335	41.66	–[a]	–	–
1	39.73	0.436	43.39	+[b]	100–430	220
1.5	88.95	1.088	45.98	+	110–440	270
2	390.5	1.137	46.31	+	160–460	280
3	–[c]	1.154	46.91	–	–	–

[a] Non-electrospinnable.
[b] Electrospinnable.
[c] The viscosity was too high to be detected at the testing shear rate of 0.01 s^{-1}.

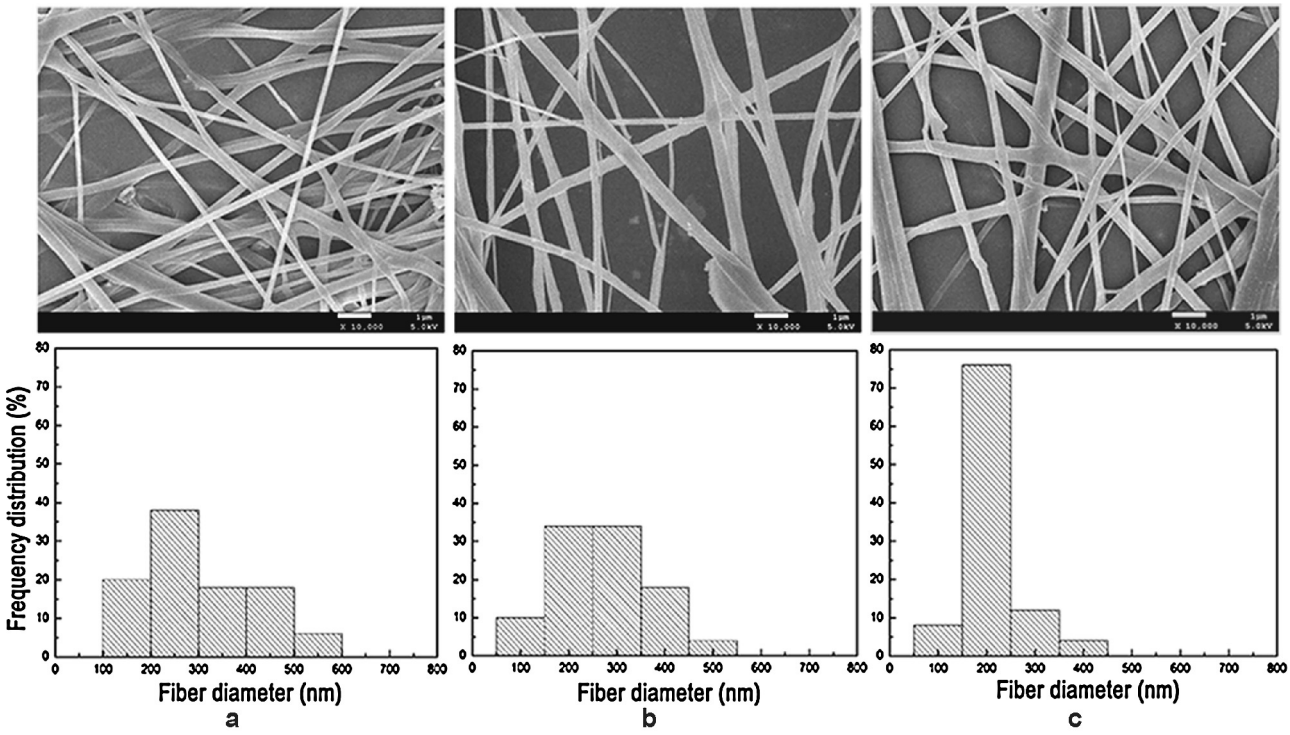

Fig. 1. SEM images and diameter distributions of electrospun cellulose nanofibers as a function of applied voltage, (a) 15 kV (b) 20 kV, and (c) 25 kV. Scale bar: 1 μm.

despite of its high conductivity, owing to the high viscosity and surface tension of the solution.

SEM was used to investigate the morphology changes of cellulose nanofibers electrospun at different applied voltages. Fig. 1 shows the typical SEM images and diameter distributions of electrospun cellulose nanofibers. The cellulose concentration was fixed at 1.5% and the tip-to-collector distance was set at 10 cm. The electrospun nonwovens were highly porous, which gave rise to high surface area to volume ratios. Distinct and uniform fiber texture could be obtained under these applied voltages. But the maximum nanofiber diameter decreased continuously with the increase of applied voltage. The average fiber diameter decreased from 300 nm to 210 nm when the applied voltage increased from 15 kV to 25 kV. In addition, narrower fiber diameter distribution was observed at 25 kV. Under certain electrospinning conditions, upon the closest approach of the electric charges, the radial force becomes stronger than the cohesive strength of the charged polymer jet. As a consequence, a single charged polymer jet splits into two or more jets (known as 'splaying') (Shukla, Brinley, Cho, & Seal, 2005). The electric charges increase when a higher voltage is applied, and the charged jet can split into more jets leading to the decrease of fiber diameter. Moreover, the increased electric field will induce a stronger stretching force upon the electrospun fibers, which makes the fibers thinner.

However, on one hand, when the applied voltage decreased to 10 kV, the cellulose solutions were no longer electrospinnable due to the weak external electric field. On the other hand, when the applied voltage increased to 30 kV, it was difficult to collect the electrospun fibers since the polymer jet on the metallic tip became very unstable.

3.2. Morphology and molecular orientation of cellulose nanofibers

Although electrospun nanofibers from native cellulose have been previously reported by several groups (Magalhães et al., 2009; Viswanathan et al., 2006; Ahn et al., 2012), very few studies, to the best of our knowledge, were focused on the morphological and structural development of electrospun cellulose nanofibers under a drawing force exerted by the collector. Also, the mechanical properties of electrospun cellulose nanofibers have rarely been evaluated before. It is expected that nanofiber and molecule orientation would remarkably influence the mechanical properties of the electrospun nonwovens. In this work, an effort has been made to explore these issues.

The morphologies of cellulose nanofibers collected at different tangential velocities of the rotating collector were shown in Fig. 2. Almost randomly oriented nanofibers were observed (Fig. 2a) when a low tangential velocity (50 m/min) was applied. This might be attributed to the bending instability of the charged jet. The fiber alignment could be significantly improved with increased tangential velocity (Fig. 2b and c). Moreover, the average fiber diameter decreased from 230 nm to 200 nm when the tangential velocity increased from 200 m/min to 300 m/min. This indicated that the nanofibers were stretched and aligned toward the drawing direction. In order to further elucidate how the electrospinning process, especially the drawing force, had modulated the structure of electrospun cellulose nanofibers, polarized FTIR, Raman spectra, and X-ray diffraction were used to analyze these materials.

The degree of molecular orientation in a stretched polymer can be evaluated using the dichroic ratio (D) (Pedicini & Farris, 2003; Kongkhlang, Tashiro, Kotaki, & Chirachanchai, 2008). Previously, Pedicini and Farris (2003) successfully employed this method to investigate the molecular orientation of electrospun polyurethane fibers. Compared with randomly aligned polyurethane fibers, a higher D value was obtained for the uniaxially aligned fibers, indicating molecular orientation could be induced by electrospinning. The D is expressed as follows: $D = A_0/A_{90}$, where A_0 is the infrared absorbance of the parallel element (0° spectrum), and A_{90} is that of the perpendicular element (90° spectrum). For a randomly oriented sample, D is equal to 1, and for a perfectly uniaxially

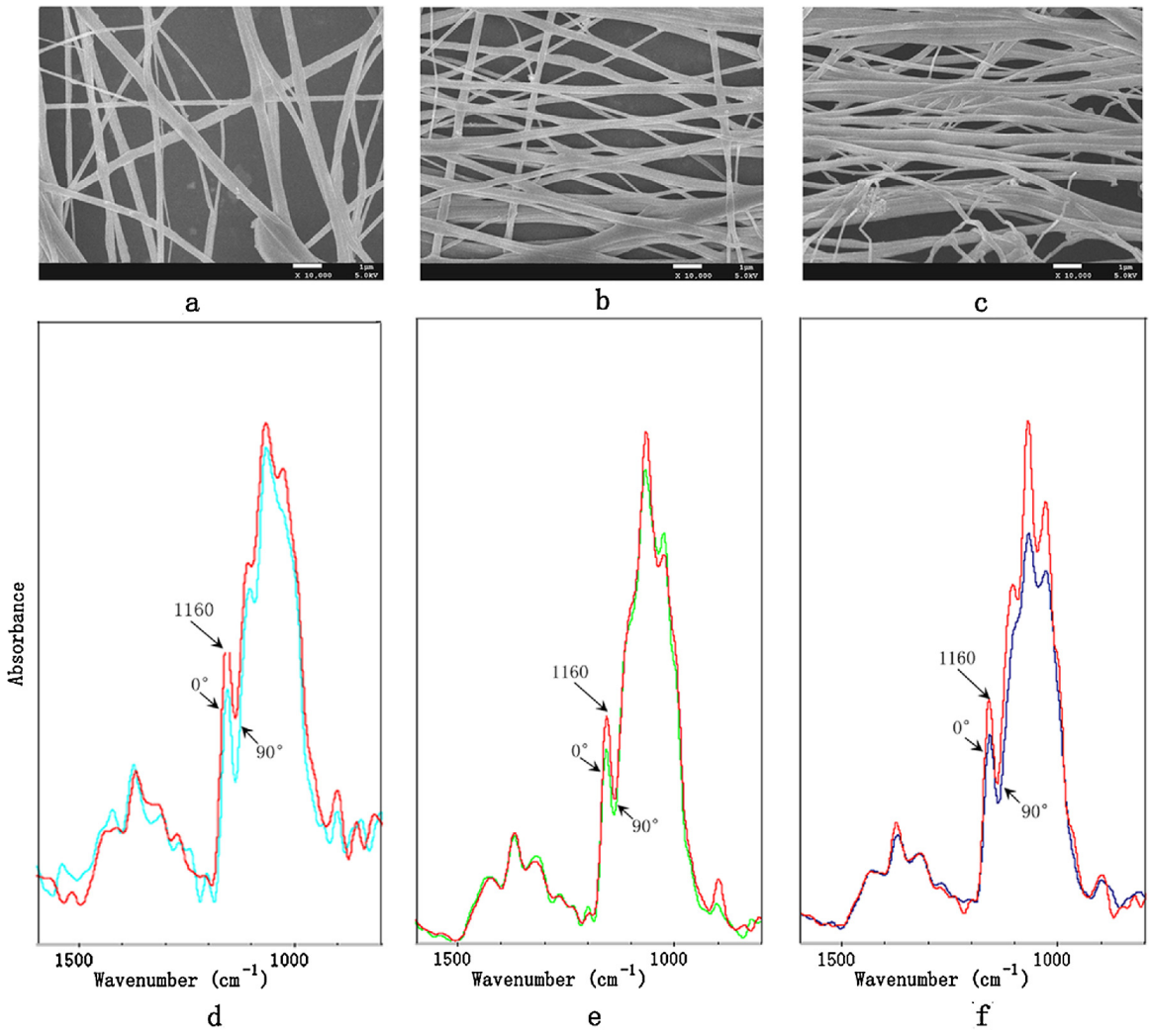

Fig. 2. Morphologies of cellulose nanofibers as a function of tangential velocity (applied voltage was 20 kV, cellulose concentration was 1.5% and the tip-to-collector distance was 10 cm), (a) 50 m/min, (b) 200 m/min, and (c) 300 m/min. Polarized FTIR transmission spectra of electrospun cellulose nanofibers collected at different tangential velocity, (d) 50 m/min, (e) 200 m/min, and (f) 300 m/min. Scale bar: 1 μm.

oriented sample (all polymer chains are oriented along the fiber axis), D is equal to infinity (Kongkhlang et al., 2008). The polarized FTIR transmission spectra of samples, which were prepared at the tangential velocity of 50 m/min, 200 m/min, and 300 m/min, were shown in Fig. 2d–f, respectively. In early work, this technique was also utilized to characterize the alignment of cellulose nanowhiskers under a magnetic field (Kimura et al., 2005). The transition moments corresponding to 1160 cm^{-1} bands assigned to the acetal linkage were parallel to the direction of cellulose chain that coincided with the long axis of the cellulose fiber (Maréchal & Chanzy, 2000; Kimura et al., 2005). In this study, it was observed that the absorbance peaks at 1160 cm^{-1} for the 0° spectrum of all samples were stronger than those for 90° spectrum (the calculated D values for the FTIR band at 1160 cm^{-1} were 1.15, 1.19, and 1.21 for the tangential velocity of 50 m/min, 200 m/min, and 300 m/min, respectively), indicating the cellulose molecules were noticeably oriented along the cellulose nanofiber axis after drawing (Maréchal & Chanzy, 2000; Kongkhlang et al., 2008). During the electrospinning process, cellulose nanofibers could suffer from a stronger drawing force if the collector rotated at a higher speed, leading to nanofiber alignment and preferential molecular orientation along the fiber axis.

3.3. Crystalline structures of cellulose nanofibers

In order to reveal the crystalline structure of electrospun cellulose, WAXD was used together with Roman spectrum. Fig. 3a shows the WAXD patterns of the pristine cotton cellulose and electrospun cellulose nanofibers obtained at different tangential velocities on the collector. The crystalline structure of cellulose remarkably changed after electrospinning. The native cellulose presented a crystalline polymorph of Type-I with the strongest scattering at $2\theta = 22.5°$, which was assigned to the [2 0 0] lattice plane. However, the electrospun nanofibers were almost amorphous, in consistent with the early work of Kim, Kim, Kang, Marquez, and Joo (2006). In addition, it was discovered that the electrospun fibers were more amorphous when collected at a higher rotating speed. During this process, the coagulation and regeneration of cellulose became very fast and there was no enough time for regular packing of cellulose chains (Baji, Mai, Wong, Abtahi, & Chen, 2010). Thus, the recrystallization of cellulose was hindered.

Raman spectra, a rapid analytical tool for analyzing the polymorphs of polymers, were used to further elucidate the crystalline structure of electrospun cellulose. As shown in Fig. 3b, cotton cellulose presented Type-I polymorph, as characterized by the six typical Raman peaks: 379, 435, 518, 904, 1095 and 1120 cm^{-1} (Schenzel &

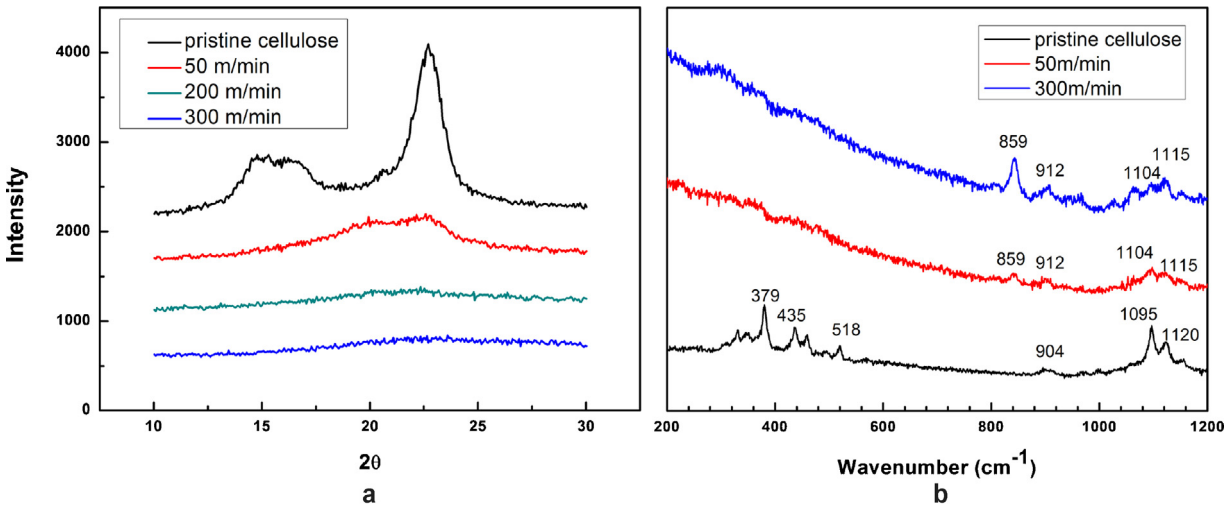

Fig. 3. (a) WAXD and (b) Raman spectra of electrospun cellulose nonwovens.

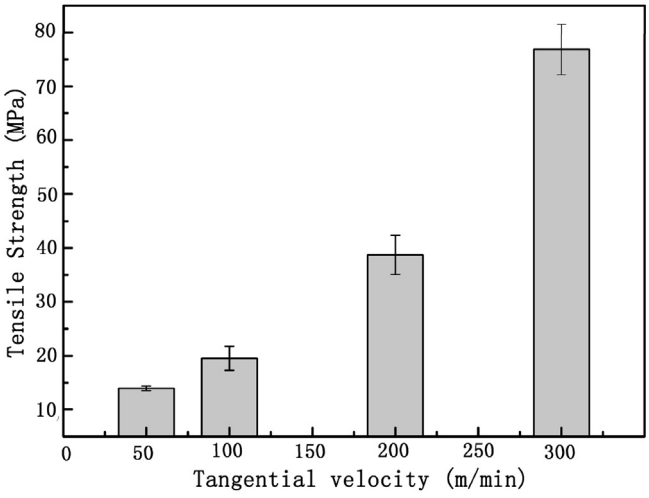

Fig. 4. Tensile strength of the electrospun cellulose nonwovens.

Fischer, 2001). However, the electrospun nanofibers showed a distinguishing polymorph as demonstrated by the peaks at 895, 912, 1104 and 1115 cm^{-1}, which were in conformity with the characteristic peaks of Type-II polymorph (Schenzel & Fischer, 2001).

The above results confirmed that cellulose nanofibers electrospun from their LiCl/DMAc solutions and coagulated with water exhibited rather low crystallinity with the polymorph of Type-II.

3.4. Tensile properties of cellulose nonwovens

For many applications including tissue engineering, the mechanical properties of electrospun nonwovens were very important for their practical usage. The mechanical deformation of electrospun nonwovens depended greatly on the alignment degree of the fibers inside (Xu, Inaic, Kotakib, & Ramakrishna, 2004; Baji et al., 2010). Fig. 4 compared the tensile strength of cellulose nonwovens fabricated at different tangential velocities on the rotating collector. Along the fiber alignment direction of the nonwovens, a significant increase of the tensile strength was recorded from 13.99 MPa (50 m/min) to 76.84 MPa (300 m/min), enhanced by 549.25%. Under tensile loading, the cellulose nanofibers inside the nonwovens could be oriented and stretched. However, only the fibers oriented along the tensile loading direction experienced the stretching force, while those fibers which oriented perpendicular to the tensile loading direction did not experience any force. Uniaxial orientation of the fibers can help equal distribution of the tensile force to all fibers. Furthermore, preferred orientation of molecular chains along the fiber long axis could favor the fiber strength as well (Wong, Baji, & Leng, 2008). It is worth to note that with the increase of fiber alignment, there should be some decrease of tensile strength in the direction perpendicular to the alignment of electrospun fibers, mainly due to the reduced number of fibers oriented in this direction.

3.5. Thermal stability of cellulose nonwovens

The thermal stability of both cotton cellulose and electrospun cellulose was analyzed by TG. The TG experiments were carried out in nitrogen atmosphere, and the results of TG and DTG were illustrated in Fig. 5. The thermal degradation of cotton cellulose initiated at 336.3 °C with the maximum thermal degradation temperature at 371.2 °C, higher than those of electrospun nanofibers. This could be ascribed to the fact that electrospun nanofibers had more contact points than raw cellulose fibers. When one nanofiber started to degrade, it could induce the thermal degradation of the surrounding nanofibers (Quiévy et al., 2010). Moreover, the highly crystalline cotton cellulose with tremendous inter- and intra-hydrogen bonding also requires more thermal energy for its degradation. Compared with cotton cellulose fibers, more carbonaceous residues were observed after thermal degradation of electrospun nanofibers. It was also noticed that the initial decomposition temperature and maximum thermal degradation temperature increased with the increase of rotating speed on the collector (279.3 °C and 318.3 °C for tangential velocity of 50 m/min vs. 287.7 °C and 330.8 °C for tangential velocity of 300 m/min). When the tangential velocity increased, more nanofibers oriented along the drawing direction, leading to fewer contact points between them and thus better thermal stability.

3.6. Morphology of hDFCs cultured on the scaffolds

Because cellulose is biocompatible and biodegradable, it is also highly hydrophilic but does not dissolve in water, the electrospun cellulose is expected to have great potentials as alternative tissue engineering scaffolds to the existing ones. To this end, cell culture studies on the eletrospun cellulose scaffolds were performed. The cell seeds used are hDFCs which were in spherical shape with diameters about 10–20 μm (Fig. 6a). The SEM images of hDFCs cultured on the scaffold (Fig. 6b) indicated that the cells could grow

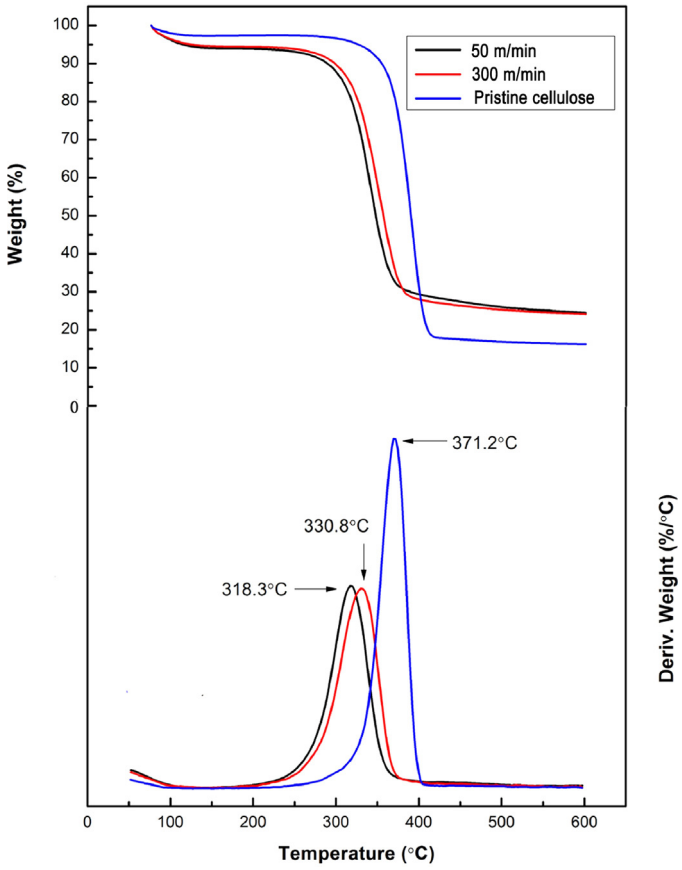

Fig. 5. TG and DTG curves of the electrospun cellulose nonwovens.

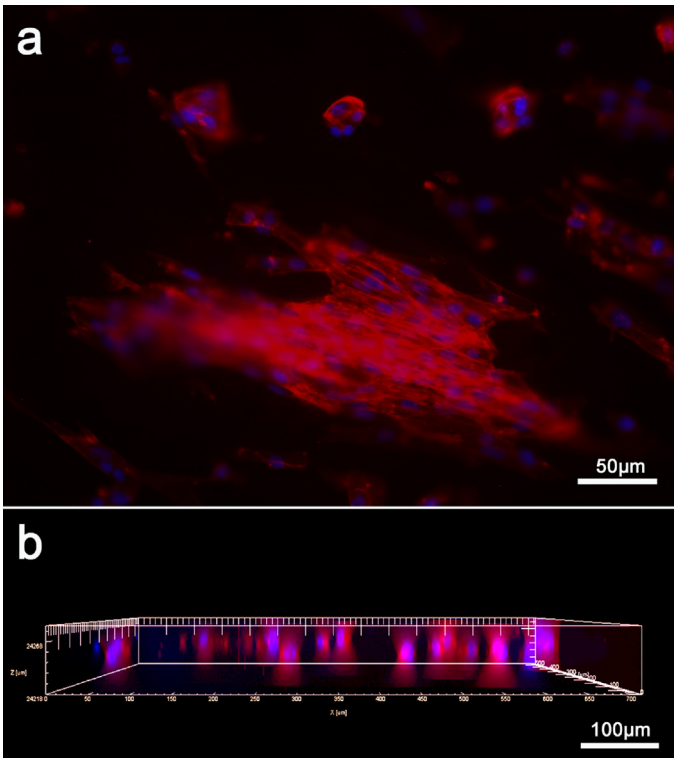

Fig. 7. (a) Confocal microscopy image of hDFCs proliferated on highly aligned cellulose nanofiber scaffolds (300 m/min), red for cell actin and blue for cell nuclei; (b) the three dimensional view of cellulose nanofibers scaffold with cells. (For interpretation of the references to color in this figure legend, the reader is referred to the web version of this article.)

and organize themselves via developing filopodia-like extensions along the nanofibers. The instrument of CLSM can give information about the physical condition of cell proliferation when seeded on the scaffold. Fig. 7a showed the CLSM image of hDFCs grown on the scaffold after 4 days culture. The cell actin (stained red) and cell nuclei (stained blue) spread well on the scaffolds. The cells were in fibril morphology with an average diameter less than 10 μm, revealing that the cells presented in Fig. 6b were actually not individual cells but cell bundles. It could also be observed that the cells inclined to interact with each other and proliferated orderly to form a confluent structure. By using Matlab software (MathWorks Co, the USA), three-dimensional reconstruction of the scaffold cultured with hDFCs could be realized. From Fig. 7b, cells seemed to have migrated into the inner part of the scaffold, showing cell related fluorescence at deeper layers. It demonstrated that hDFCs could proliferate well in the entire scaffold. When the cell seeds proliferated on the scaffold, on one hand, cells could form pseudopodia and change their shape into oval to pass through the narrow pores by amoeboid movement. Pseudopodia are protrusions of cytoplasm of the cell which help cells move forward in a crawling-like type of movement (Margheri et al., 2014). On the other hand, as anchorage-dependent cells, hDFCs would spread after being attached on the scaffold (Yost et al., 2000). Consequently, it is possible for hDFCs to

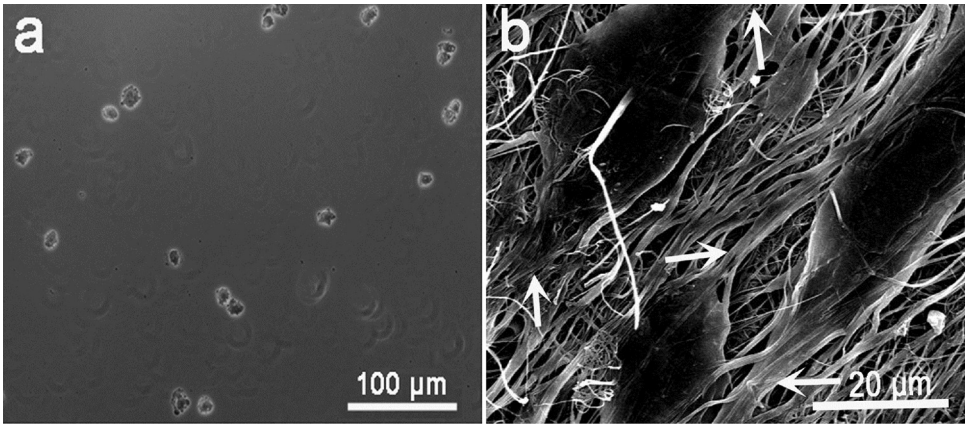

Fig. 6. (a) Optical microscopy image of the hDFCs seeds. (b) SEM image of hDFCs cultured on electrospun cellulose nanofiber scaffolds. Arrows point to fiber-guided filopodia-like cell extensions.

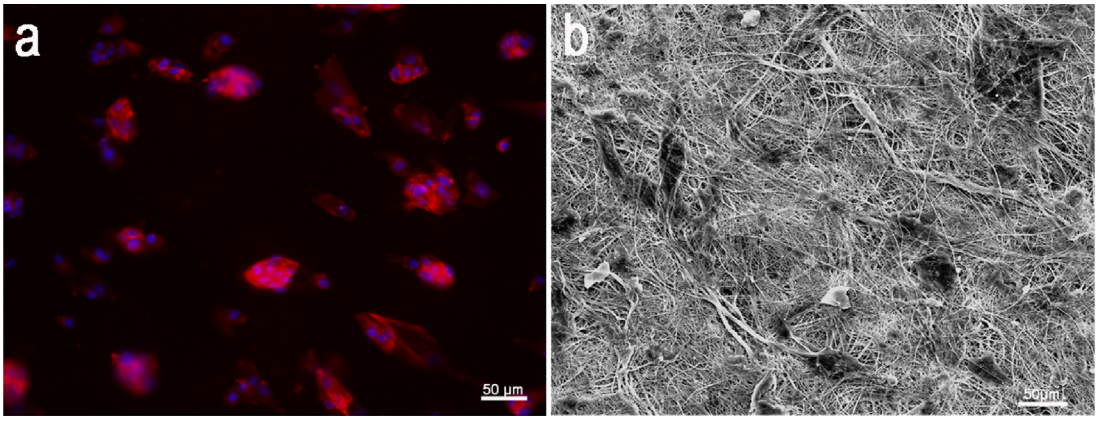

Fig. 8. hDFCs proliferated on randomly aligned cellulose nanofiber scaffolds (collected at 50 m/min), (a) CLSM image and (b) SEM image.

penetrate into the inner part of the scaffold through the massive pores in the electrospun scaffold rather than merely grown on the scaffold's surface.

For comparison, studies were also done on randomly aligned scaffolds. It is clear that cells could only be attached to and randomly scattered on the scaffold (Fig. 8). A highly confluent cell structure similar to that on uniaxially aligned scaffold could hardly be achieved. A possible reason for this might be that aligned nanofibers retain fibroblast natural ECM structure which is more favorable for cell adhesion and proliferation than randomly aligned scaffold (Lee et al., 2005).

It is important to note that no surface modification was applied for the electrospun cellulose nanofibers, but experimentally very good cell adhesion and spreading were observed. The MTT assays (data not shown) indicated the OD (optical density) values of electrospun native cellulose over all the testing days, especially the highly aligned ones, are even higher than those of positive control. Also, compared with some of the most commonly used electrospun scaffold materials, namely, cellulose acetate and PLGA, the OD values of our scaffold were distinctly higher, suggesting the high biocompatibility and bioactivity. The unique amorphous cellulose content of present scaffolds presumably allowed their excellent biocompatibility and bioactivity. Investigation is still underway and will be reported later.

4. Conclusion

The present study systematically investigated the key factors influencing the electrospinning process of native cellulose in its LiCl/DMAc solutions. A rotating collector with a water coagulation bath was adopted to fabricate well aligned cellulose nanofibers. The nanofibers produced under the optimal conditions exhibited distinct and uniform fiber texture. The alignment and the molecular orientation of the electrospun nanofibers were strengthened when a higher tangential velocity was applied on the collector. From WAXD together with Roman spectra, it was confirmed that the electrospun cellulose nanofibers were almost amorphous. Remarkable enhancements of tensile strength and thermal stability of the electrospun nonwovens were achieved by increasing the tangential velocity. Cell culture experiments demonstrated the highly aligned electrospun scaffold was quite suitable for hDFCs attachment and proliferation in the entire scaffold. This study showed that the electrospun cellulose nanofiber nonwovens with excellent physicochemical properties have great potential as scaffold materials in tissue engineering.

Acknowledgements

The authors would like to thank National Natural Science Foundation of China (51303112, 51473100 and 51433006) for financial support of this work.

References

Ahn, Y., Lee, S. H., Kim, H. J., Yang, Y. H., Hong, J. H., Kim, Y.-H., et al. (2012). Electrospinning of lignocellulosic biomass using ionic liquid. *Carbohydrate Polymers*, *88*, 395–398.

Baji, A., Mai, Y. W., Wong, S. C., Abtahi, M., & Chen, P. (2010). Electrospinning of polymer nanofibers: Effects on oriented morphology structures and tensile properties. *Composites Science and Technology*, *70*, 703–718.

Bhat, S., & Kumar, A. (2012). Cell proliferation on three-dimensional chitosan–agarose–gelatin cryogel scaffolds for tissue engineering applications. *Journal of Bioscience and Bioengineering*, *114*, 663–670.

Blond, D., Walshe, W., Young, K., Blighe, F. M., Khan, U., Almecija, D., et al. (2008). *Advanced Functional Materials*, *18*(2), 618–2624.

Czaja, W. K., Young, D. J., Kawecki, M., & Brown, R. M. (2007). The future prospects of microbial cellulose in biomedical applications. *Biomacromolecules*, *8*, 1–12.

Dupont, A. L. (2003). Cellulose in lithium chloride/*N*,*N*-dimethylacetamide optimisation of a dissolution method using paper substrates and stability of the solutions. *Polymer*, *44*, 4117–4126.

Du, J., & Hsieh, Y. L. (2009). Cellulose/chitosan hybrid nanofibers from electrospinning of their ester derivatives. *Cellulose*, *16*, 247–260.

Frey, M. W. (2008). Electrospinning cellulose and cellulose derivatives. *Polymer Reviews*, *48*, 378–391.

Fricain, J. C., Granja, P. L., Barbosa, M. A., deJéeso, B., Barthe, N., Baquey, C., et al. (2002). Cellulose phosphates as biomaterials in vivo biocompatibility studies. *Biomaterials*, *23*, 971–980.

Greiner, A., & Wendorf, J. H. (2007). Electrospinning: A fascinating method for the preparation of ultrathin fibers. *Angewandte Chemie International Edition*, *46*, 5670–5703.

Hon, D. N. S. (1994). Cellulose: A random walk along its historical path. *Cellulose*, *1*, 1–25.

Jayaramudu, J., Siva Mohan Reddy, G., Varaprasad, K., Sadiku, E. R., Sinha Ray, S., Varada Rajulu, A., et al. (2013). Preparation and properties of biodegradable films from *Sterculia urens* short fiber/cellulose green composites. *Carbohydrate Polymers*, *93*, 622–627.

Jose, M. V., Thomas, V., Johnson, K. T., Dean, D. R., & Nyairo, E. (2009). Aligned PLGA/HA nanofibrous nanocomposite scaffolds for bone tissue engineering. *Acta Biomaterialia*, *5*, 305–315.

Kim, C. W., Kim, D. S., Kang, S. Y., Marquez, M., & Joo, Y. L. (2006). Structural studies of electrospun cellulose nanofibers. *Polymer*, *47*, 5097–5107.

Kimura, F., Kimura, T., Tamura, M., Hirai, A., Ikuno, M., Horii, F., et al. (2005). Magnetic alignment of the chiral nematic phase of a cellulose microfibril suspension. *Langmuir*, *21*, 2034–2037.

Kongkhlang, T., Tashiro, K., Kotaki, M., & Chirachanchai, S. (2008). Electrospinning as a new technique to control the crystal morphology and molecular orientation of polyoxymethylene nanofibers. *Journal of the American Chemical Society*, *130*, 15460–15466.

Lee, C. H., Shin, H. J., Cho, I. H., Kang, Y. M., Kim, I., Park, K. D., et al. (2005). Electrospun fine-textured scaffolds for heart tissue constructs. *Biomaterials*, *26*, 1261–1270.

Ma, M. G., Qing, S. J., Li, S. M., Zhu, J. F., Fu, L. H., Sun, R. C., et al. (2013). Microwave synthesis of cellulose/CuO nanocomposites in ionic liquid and its thermal transformation to CuO. *Carbohydrate Polymers*, *91*, 162–168.

Magalhães, W. L. E., Cao, X., & Lucia, L. A. (2009). Cellulose nanocrystals/cellulose core-in-shell nanocomposite assemblies. *Langmuir*, *25*, 13250–13257.

Mahmoudian, S., Wahit, M. U., Ismail, A. F., & Yussuf, A. A. (2012). Preparation of regenerated cellulose/montmorillonite nanocomposite films via ionic liquids. *Carbohydrate Polymers*, *88*, 1251–1257.

Margheri, F., Luciani, C., Taddei, M. L., Giannoni, E., Laurenzana, A., Biagioni, A., et al. (2014). The receptor for urokinase-plasminogen activator (uPAR) controls plasticity of cancer cell movement in mesenchymal and amoeboid migration style. *Oncotarget*, http://www.ncbi.nlm.nih.gov/pubmed/24681666.

Maréchal, Y., & Chanzy, H. (2000). The hydrogen bond network in I_β cellulose as observed by infrared spectrometry. *Journal of Molecular Structure*, *523*, 183–196.

Morsczeck, C., Götz, W., Schierholz, J., Zeilhofer, F., Kühn, U., Möhl, C., et al. (2005). Isolation of precursor cells (PCs) from human dental follicle of wisdom teeth. *Matrix Biology*, *24*, 155–165.

Müller, F. A., Müller, L., Hofmann, I., Greil, P., Wenzel, M. M., Staudenmaier, R., et al. (2006). Cellulose-based scaffold materials for cartilage tissue engineering. *Biomaterials*, *27*, 3955–3963.

Nishio, Y. (2006). Material functionalization of cellulose and related polysaccharides via diverse microcompositions. *Advances in Polymer Science*, *205*, 97–151.

Pedicini, A., & Farris, R. J. (2003). Mechanical behavior of electrospun polyurethane. *Polymer*, *44*, 6857–6862.

Potthast, A., Rosenau, T., Buchner, R., Röder, T., Ebner, G., Bruglachner, H., et al. (2002). The cellulose solvent system *N,N*-dimethylacetamide/lithium chloride revisited: The effect of water on physicochemical properties and chemical stability. *Cellulose*, *9*, 41–53.

Quiévy, N., Jacquet, N., Sclavons, M., Deroanne, C., Paquot, M., Devaux, J., et al. (2010). Influence of homogenization and drying on the thermal stability of microfibrillated cellulose. *Polymer Degradation and Stability*, *95*, 306–314.

Reneker, D. H., & Yarin, A. L. (2008). Electrospinning jets and polymer nanofibers. *Polymer*, *49*, 2387–2425.

Rnjak-Kovacina, J., Wise, S. G., Li, Z., Maitz, P. K. M., & Young, C. J. (2011). Tailoring the porosity and pore size of electrospun synthetic human elastin scaffolds for dermal tissue engineering. *Biomaterials*, *32*, 6729–6736.

Rodríguez, K., Gatenholm, P., & Renneckar, S. (2012). Electrospinning cellulosic nanofibers for biomedical applications: Structure and in vitro biocompatibility. *Cellulose*, *19*, 1583–1598.

Schenzel, K., & Fischer, S. (2001). NIR FT Raman spectroscopy—A rapid analytical tool for detecting the transformation of cellulose polymorphs. *Cellulose*, *8*, 49–57.

Schiffman, J. D., & Schauer, C. L. (2008). A review: Electrospinning of biopolymer nanofibers and their applications. *Polymer Reviews*, *48*, 317–352.

Sehaqui, H., Morimune, S., Nishino, T., & Berglund, L. A. (2012). Stretchable and strong cellulose nanopaper structures based on polymer-coated nanofiber networks: An alternative to nonwoven porous membranes from electrospinning. *Biomacromolecules*, *13*, 3661–3667.

Shukla, S., Brinley, E., Cho, H. J., & Seal, S. (2005). Electrospinning of hydroxypropyl cellulose fibers and their application in synthesis of nano and submicron tin oxide fibers. *Polymer*, *46*, 12130–12145.

Sill, T. J., & von Recum, H. A. (2008). Electrospinning: Applications in drug delivery and tissue engineering. *Biomaterials*, *29*, 1989–2006.

Suwantong, O., Opanasopit, P., Ruktanonchai, U., & Supaphol, P. (2007). Electrospun cellulose acetate fiber mats containing curcumin and release characteristic of the herbal substance. *Polymer*, *48*, 7546–7557.

Thomas, V., Jose, M. V., Chowdhury, S., Sullivan, J. F., Dean, D. R., Vohra, Y. K., et al. (2006). Mechano-morphological studies of aligned nanofibrous scaffolds of polycaprolactone fabricated by electrospinning. *Journal of Biomaterials Science, Polymer Edition*, *17*, 969–984.

Viswanathan, G., Murugesan, S., Pushparaj, V., Nalamasu, O., Ajayan, P. M., Linhardt, R. J., et al. (2006). Preparation of biopolymer fibers by electrospinning from room temperature ionic liquids. *Biomacromolecules*, *7*, 415–418.

Wang, W., Zhang, P., Zhang, S., Li, F., Yu, J., Lin, J., et al. (2013). Structure and properties of novel regenerated cellulose fibers prepared in NaOH complex solution. *Carbohydrate Polymers*, *98*, 1031–1038.

Wong, S.-C., Baji, A., & Leng, S. (2008). Effect of fiber diameter on tensile properties of electrospun poly(3-caprolactone). *Polymer*, *49*, 4713–4722.

Xu, C. Y., Inaic, R., Kotakib, M., & Ramakrishna, S. (2004). Aligned biodegradable nanofibrous structure: A potential scaffold for blood vessel engineering. *Biomaterials*, *25*, 877–886.

Yost, M. J., Simpson, D., Wrona, K., Ridley, S., Ploehn, H. J., Borg, T. K., et al. (2000). Design and construction of a uniaxial cell stretcher. *American Journal of Physiology: Heart and Circulatory Physiology*, *9*, H3124–H3130.